Comparative analysis on the magnetite deposition behavior of Alloy 600 and Alloy 690 in secondary system of PWRs

Soon-Hyeok Jeon[a,*], Yong-Beom Lee[a,b], Do Haeng Hur[a]
[a]*Materials Safety Technology Development Division, Korea Atomic Energy Research Institute, 989-111, Daedeok-daero, Yuseong-gu, Daejeon, 34057, Republic of Korea*
[b]*Department of Materials Science and Engineering, Chungnam National University, 99, Daehak-ro, Yuseong-gu, Daejeon, 34134, Republic of Korea*
[*]*Corresponding author: junsoon@kaeri.re.kr*

Introduction

In pressurized water reactors (PWRs), many structural components such as control rod drive mechanism (CRDM) nozzles, steam generator (SG) tube, and SG divider plates are made of Ni-based alloys. These components were initially made of Alloy 600 because it had exhibited a good corrosion resistance in many aggressive environments. However, Alloy 600 was found to be susceptible to stress corrosion cracking (SCC) in primary coolant system, having a case reported in field in 1971 after only two years in service and is still being occurred in field [1].

Alloy 690 with a higher Cr content of about 30% in weight was newly developed as an alternative to solve the SCC problem of Alloy 600. After that, many researchers studied to compare the SCC susceptibility of Alloy 600 and Alloy 690 and showed that Alloy 690 has an excellent SCC resistance than that of Alloy 600 in various environments. Due to the excellent SCC resistance of Alloy 690, Alloy 690 thermally treated (TT) SG tube has been used in many operating plants since 1988, and no cracking owing to SCC has been reported to date [2,3].

In the respective of SG integrity of PWRs, not only the SCC susceptibility of SG tube but also magnetite deposition behavior is very important. In secondary coolant system, magnetite formed in the feedwater piping, condensate, and the drain systems is transported into SG and deposited on the surfaces of SG tubes [4,5]. Magnetite deposited on the surface of SG tube could decrease the heat transfer efficiency and interfere with the SG hydrodynamics. Furthermore, various aggressive impurities such as Pb, S, and Cl could concentrate in porous magnetite deposits [6-8] and thus accelerate the corrosion rate of SG components [8]. Therefore, reducing the magnetite deposits is a crucial factor to improve the integrity of SG. However, there has been no study on the comparative analysis on the magnetite deposition of Alloy 600 and Alloy 690 in secondary system of PWRs. Especially, the comparative analysis on the porosity of magnetite deposited on the Alloy 600 and Alloy 690 is not studied.

In this paper, we investigated the effect of Cr content on magnetite deposition behavior of SG tubes in a secondary water system of PWRs. The surface and cross-section of magnetite deposits were observed. Porosity of magnetite deposits were also compared. After the chemical cleaning for magnetite deposits, the Fe content of the deposits is measured and total amount of deposits is calculated by addition of O. To elucidate the mechanism of magnetite deposition behavior, zeta potential of magnetite and surface roughness and surface zeta potential of SG tubes were measured in simulated secondary water.

2. Experimental methods

Fig. 1 shows a photo of the magnetite deposition loop system that could simulate the secondary water conditions of the SG in PWRs. the deposition loop system composed of four main parts: a temperature controller, a test section installed with a SG tube specimen, a water tank filled with deionized water, and a Fe source tank filled with Fe acetate solution. Commercial SG tubes (Alloy 600 and Alloy 690) were used as the test specimens. The dimensions of the tubes were outer diameter (OD) of 19.05 mm, inner diameter (ID) of 17.00 mm and length of 500 mm.

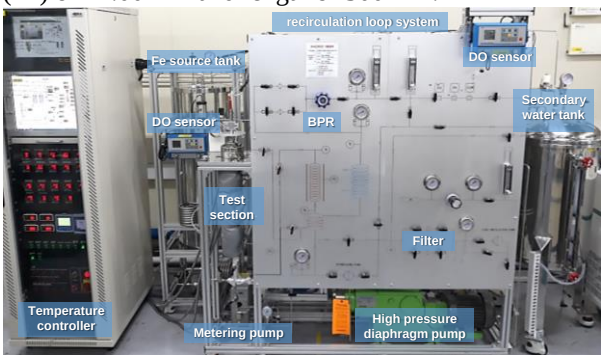

Fig. 1. Photo of recirculation secondary loop system for magnetite deposition test.

In this loop system, the flow rate of secondary water was continued at 260 ml/min and the dissolved oxygen (DO) content was continued below 5 ppb. The pH value of the water was sustained at 10.0 by injecting diluted solutions of ETA, and the pH value was monitored using an in situ pH sensor. When the loop system was ready to start, the pressure of test section was then increased to 60 bar by the BPR, and the water temperature near the tube surface was maintained at about 270 ºC to occur subcooled nucleate boiling (SNB) by operating the pre-heater, ceramic heaters surrounding

the test section, and the internal heater inside the SG tube. The heat flux of the internal heater was continued at about 30 W/cm^2.

After these test conditions were set, we injected the Fe ions into the test section through the injection pump with a flow rate of 1 ml/min from the Fe source tank. The precursor solution was diluted in the simulated secondary water and its final content was calculated as 1 ppm Fe in the test section. The magnetite deposition test was conducted for 14 days without shutdown.

After the deposition test, the specimens were cut using a low-speed diamond saw. As shown in Fig. 2, three types of specimens were fabricated to conduct various analyses. First, three tubular specimens with a 20 mm length were used to measure the amount of magnetite deposition. To measure the amounts of deposition, the magnetite deposits were selectively dissolved by immersing them in a chemical cleaning solution (20 wt.% ethylenediaminetetraacetic (EDTA) acid + 1 wt.% N_2H_4 + 1 wt.% corrosion inhibitor + NH_4OH) at 93 ºC for 12 h. The dissolved solutions were directly analyzed using an inductively coupled plasma atomic emission spectroscope (ICP-AES) to measure the Fe content. Finally, the total amount of magnetite deposition per unit area was converted to magnetite using the measured Fe content. Second, the two tubular specimens of 15 mm long were used to analyze the particle morphologies and characteristics. The surface morphologies of the deposits were observed using a scanning electron micro-scope (SEM). Two-dimensional particle characteristics and distribution of the deposits was evaluated using an image analyzer. Third, four tubular specimens of 10 mm long were used to analyze the porosity of deposits. Cross sections of the deposits were prepared using the focused ion beam (FIB) technique, and three locations per specimen were observed using FIB-SEM. The two-dimensional porosity of the deposits was also evaluated using an image analyzer. It was used to analyze four images per location (i.e., at least 12 images per specimen) for each analysis using a cross-sectional SEM images.

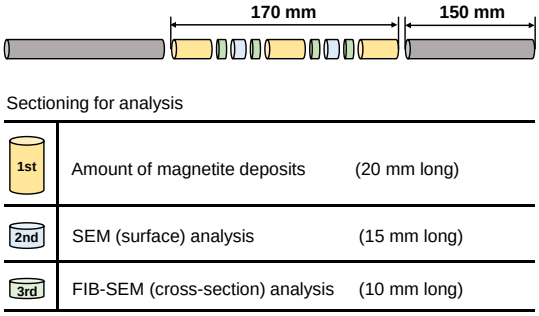

Fig. 2. Three sections of an SG tube specimens for analysis after the magnetite deposition test.

The zeta potentials of magnetite nanoparticles and the surface of SG tubes (Alloy 600 and Alloy 690) were measured at 25 ºC. To measure the zeta potentials of the magnetite particles, we prepared samples by dispersing 5 nm magnetite nanoparticles in deionized water at a concentration of 25 mg/l. Diluted ETA was added to the sample, whose pH value was set at 10.0, and the prepared sample was transferred to a zeta potential measurement cell. After then, the Zetasizer applied an electric field to the sample through an electrode fixed to the cell. The magnetite nanoparticles moved toward the electrode depending on their charge, and the electrophoretic mobility was proportional to the intensity of the electric field and the zeta potential of the magnetite particles. By using the electrophoretic light scattering, the Zetasizer measured the electrophoretic mobility of the magnetite particles and then measured the zeta potential of particle from Henry's equation (Fig. 3 (a)). The surface zeta potential of alloy steels could be estimated by measuring the electrophoretic mobility at several distances from the specimen surface using a suspended particle tracer. The prepared sample was stuck to the specimen holder and immersed in the cuvette solution. This solution was the same condition for measuring the magnetite particles.

Supplying an electric field through a pair of Pd electrodes started electrophoresis of the tracer particles. Electrical effects of the tracer measurements were conducted at four different distances (0, 90, 180, 270 degree) from the sample surface by rotating a screw to vary the sample height (Fig 3 (b)). The surface zeta potential of each Alloy 600 and 690 plates was obtained by linear extrapolation.

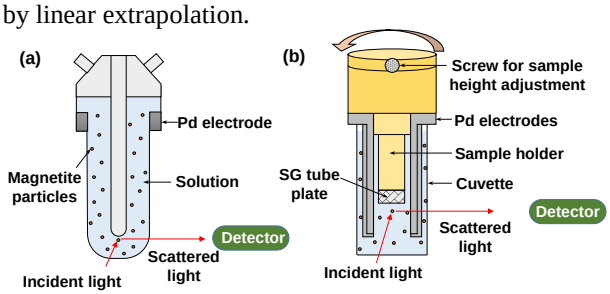

Fig. 3. Schematic of (a) Particle zeta potential kit and (b) Surface zeta potential kit.

Not only zeta potential but also surface roughness of SG tubes is very important factor for the magnetite deposition behavior. Hence, the surface roughness of Alloy 600 and Alloy 690 were measured using a non-contacting surface profiler at least three times to confirm the reproducibility. We confirmed that the roughness of surface of both SG tubes (Alloy 600 and Alloy 690) were almost same value (R_a: 0.20~0.21 μm).

3. Results and Discussion

3.1. Microstructural analysis of SG tube deposits

Fig. 4 (a) shows the SEM micrographs of the surface of magnetite deposited onto the Alloy 600 and Alloy 690 tubes. Regardless of Cr content of the SG tubes, the

magnetite particles were polyhedral or spherical in shape with a size of several tens of nanometers to several micrometers, which is almost similar to the actual SG tube deposits in field. In addition, extremely small pores could be observed between the magnetite particles. Based on the SEM images, the Cr content of SG tubes do not seem to have a significant effect on the morphology of the magnetite particles.

Fig. 4 (b) shows the cross-sectional FIB-SEM images of the magnetite deposits of both SG tubes. Numerous micro-pores with diameter between about 0.1 μm and 10 μm were clearly observed in the magnetite deposits under all SG tubes. They were formed when steam bubbles escaped from the heated SG tube surface.

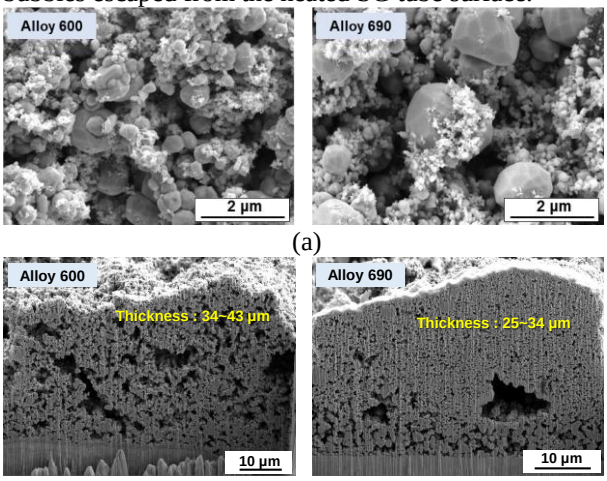

Fig. 4. SEM images of the surface and cross-section of magnetite deposited on SG tubes: (a) surface and (b) cross-section.

Fig. 5 shows the porosity of the magnetite deposits on Alloy 600 and Alloy 690 tubes as determined using an image analyzer and FIB-SEM images. The porosity of Alloy 600 was larger than that of Alloy 690. We think that the difference in porosity between Alloy 600 and Alloy 690 may affect the heat transfer efficiency of the SG tube deposited magnetite during the operation of PWRs.

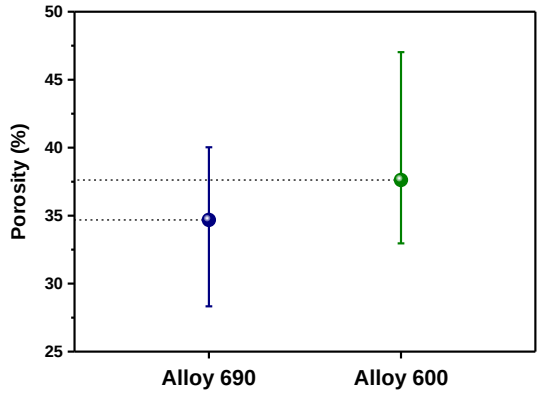

Fig. 5. Porosity of magnetite deposits on SG tubes as determined using an image analyzer.

3.2. The amount of magnetite deposition

Fig. 6 shows the amount of magnetite per unit area deposited onto the SG tubes. The results indicates that Cr content of SG tubes clearly affect the amount of magnetite deposits. The amount of magnetite deposits in high, middle, low positions of Alloy 600 increased about 16%, 37%, and 30% than those of Alloy 690, respectively. Although slightly different for each position, the average amount of magnetite deposits in the case of Alloy 600, compared to Alloy 690, increased about 28%.

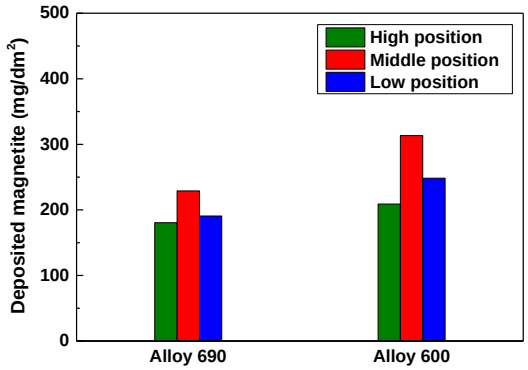

Fig. 6. The amount of magnetite per unit area deposited onto the SG tubes depending on the pH control agents and pH values.

Fig. 7 shows the zeta potentials of both magnetite nanoparticles and the surface of Alloy 600 and Alloy 690 plates at 25 ℃. Under all SG tubes, both the particles and plate surfaces have the negative charge values, showing that the force that worked between them was a repulsive force. The difference in zeta potentials between the particle and the surface of Alloy 600 and Alloy 690 was 2.9 mV and 6.5 mV, respectively. Hence, in the initial stage of magnetite deposition, the amount of magnetite deposited on the Alloy 690 specimen surface decreased due to the larger difference in zeta potential between the magnetite particles and the plate surface, compared to Alloy 600.

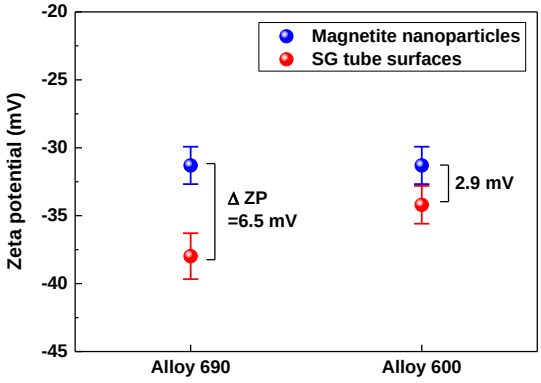

Fig. 7. Zeta potentials at 25 ºC of the surface of Alloy 600 and Alloy 690 plate and magnetite nanoparticles.

4. Conclusions

(1) Regardless of Cr content of the SG tubes, the deposited-magnetite particles were polyhedral or spherical in shape. Numerous micro-pores were clearly observed in the deposits.

(2) The porosity of magnetite on Alloy 600 was larger than that on Alloy 690. The difference in porosity may affect the heat transfer efficiency of the SG tube in operation. In addition, the average amount of magnetite deposits on Alloy 600 increased about 28% compared to that on Alloy 690.

(3) Based on the results, zeta potential of SG tubes seem to have a significant effect on the magnetite deposition behavior. Compare with Alloy 600, Alloy 690 not only has the excellent SCC resistance, but also has less the magnetite deposits.

Acknowledgement

This work was supported by the National Research Foundation (NRF) grant of the Republic of Korea funded by the Korean government (NRF-2017M2A8A4015159).

REFERENCES

[1] J. Hickling, C. King, Materials Reliability Program (MPR), Resistance to Primary Water Stress Corrosion Cracking of Alloys 690, 52, and 152 in Pressurized Water Reactors (MPR-111), EPRI, Palo Alto, CA. USA (EPRI report 1009801), 2004.
[2] K. Stiller, J.O. Nilsson, K. Norring, Structure, chemistry, and stress corrosion cracking of grain boundaries in alloys 600 and 690, Metal. Mater. Trans. A. 27, 327-341, 1996.
[3] T. Yonezawa, K. Onimura, N. Sasaguri, T. Kusakabe, H. Nagano, K. Yamanaka, T. Minami, M. Inoue, Effects of heat treatment on corrosion resistance of Alloy 690, in Proceedings of the 2nd International Symposium on Environmental Degradation of Materials in Nuclear Power Systems-Water Reactors, pp. 593-600, Calif, USA, September 1985.
[4] C. Ramesh, N. Murugesan, A.A.M. Prince, S. Velmurugan, S.V. Narasimhan, V. Ganesan, Application of polymer electrolyte based hydrogen sensor to study corrosion of carbon steel in acid medium, Corros. Sci. 43, 1865-1875, 2001.
[5] A.A.M. Prince, S. Velmurugan, S.V. Narasimhan, C. Ramesh, N. Murugesan, R.S. Raghavan, R.J. Gopalan, Dissolution behavior of magnetite film formed over carbon steel in dilute organic acid media, J. Nucl. Mater. 289, 281-290, 2001.
[6] J.P.N. Paine, S.A. Hobart, S.G. Sawochka, Predicting steam generator crevice chemistry. In Proceedings of the 5th International Symposium on Environmental Degradation of Materials in Nuclear Power System-Water Reactors, Monterey, CA, USA, 25-29 August, 739-744, 1991.
[7] P.J. Millet, J.M. Fenton, A detailed model of localized concentration processes in porous deposits of SGs. In Proceedings of the 5th International Symposium on Environmental Degradation of Materials in Nuclear Power System-Water Reactors, Monterey, CA, USA, 25-29 August, 745-751, 1991.
[8] T. Sakai, T. Senjuh, K. Aoki, T. Shigemitsu, Y. Kishi, Lead induced stress corrosion cracking of Alloy 600 and 690 in high temperature water. In Proceedings of the 5th International Symposium on Environmental Degradation of Materials in Nuclear Power System-Water Reactors, Monterey, CA, USA, 25-29 August, 764-772, 1991.